International Journal of Minerals, Metallurgy and Materials
Volume 23, Number 12, December 2016, Page 1458
DOI: 10.1007/s12613-016-1370-5

Thermodynamic simulation of the effect of slag chemistry on the corrosion behavior of alumina–chromia refractory

Shi-xian Zhao[1)], *Bin-li Cai*[1)], *Hong-gang Sun*[1)], *Gang Wang*[1)], *Hong-xia Li*[1)], *and Xiao-yan Song*[2)]

1) State Key Laboratory of Advanced Refractories, Sinosteel Luoyang Institute of Refractories Research Co., Ltd., Luoyang 471039, China
2) School of Materials Science and Engineering, Beijing University of Technology, Beijing 100124, China
(Received: 20 July 2016; revised: 9 September 2016; accepted: 12 September 2016)

Abstract: The corrosion behavior of alumina–chromia refractory against two kinds of industrial slags (coal slag and iron smelting slag) at 1550°C was investigated via thermodynamic simulations. In the proposed simulation model, the initial slag first attacks the matrix and surface aggregates and subsequently attacks the inner aggregates. The simulation results indicate that the slag chemistry strongly affects the phase formation and corrosion behavior of the refractory brick. Greater amounts of alumina were dissolved and spinel solid phases formed when the brick interacted with iron smelting slag. These phenomena, as well as the calculated lower viscosity, may lead to much deeper penetration than that exhibited by coal slag and to more severe corrosion compared to that induced by coal slag. The thermodynamic calculations well match the experimental observations, demonstrating the efficiency of the proposed simulation model for evaluating the corrosion behavior of alumina–chromia refractory.

Keywords: thermodynamic analysis; simulation; corrosion; spinel; alumina; chromia; refractories

1. Introduction

Alumina–chromia refractory is a heterogeneous material that contains a certain amount of chromia, which substantially improves the wear resistance of bricks compared to the wear resistance of alumina bricks because of the formation of an Al_2O_3–Cr_2O_3 solution [1–2]. Because of this advantage, alumina–chromia refractory bricks have been widely used as a lining material in various types of high-temperature furnaces for years [3–5]. However, because of the complex environmental conditions in the furnaces at operating temperature, the alumina–chromia refractory is simultaneously subjected to severe chemical and mechanical corrosion. Generally, molten slag attack is assumed to be the primary cause of corrosion, and the composition of the molten slag critically affects the corrosion mechanisms of the brick. Numerous relevant studies have been reported, most of which have involved experimental tests [6–9]. An alternative approach to understanding the reaction and corrosion mechanisms of alumina–chromia refractory brick is through thermodynamic simulations.

Thermodynamic simulations are particularly suitable for elucidating corrosion phenomena. They provide information about the formed phases, their proportions and compositions, the chemical activities of individual components, and the thermodynamic properties of the various compositions at different partial pressures and temperatures [10]. By analyzing the equilibrium reactions, investigators can gain better knowledge of the corrosion mechanisms, which is useful for improving industrial performance, thereby reducing the need for experimental tests [11].

Research on predicting refractory corrosion behavior using thermodynamic models has recently been reported [12–16]. However, some important factors, such as the difference between the matrix and aggregate compositions in refractory materials and the change in chemical composition of slag after the reaction with the refractory, were not considered or were only partially considered in these works.

This work addresses the thermodynamic simulation of the corrosion behavior of alumina–chromia refractory brick

Corresponding author: Shi-xian Zhao E-mail: andyzhaosx@163.com

against two slags of industrial composition; the developed model first considers the reaction with the matrix and then that with the aggregates when molten slag is in contact with the refractory brick. The changes in slag composition during the interaction are also considered in the proposed simulation process. Moreover, to evaluate the corrosion mechanisms and demonstrate the advantages of thermodynamic simulations, we conducted experimental corrosion tests and compared the results with those attained by calculations.

2. Experimental and thermodynamic modeling

2.1. Alumina–chromia refractory brick composition

The alumina–chromia refractory brick used in this work was commercially sintered refractory with a composition of 88wt% Al_2O_3 and 12wt% Cr_2O_3. Fig. 1 presents a scanning electron microscopy (SEM) micrograph of the refractory brick, which comprised two clearly distinct regions: the Al_2O_3 aggregates (dark regions) and the matrix containing 70wt% Al_2O_3 and 30wt% Cr_2O_3 (bright regions).

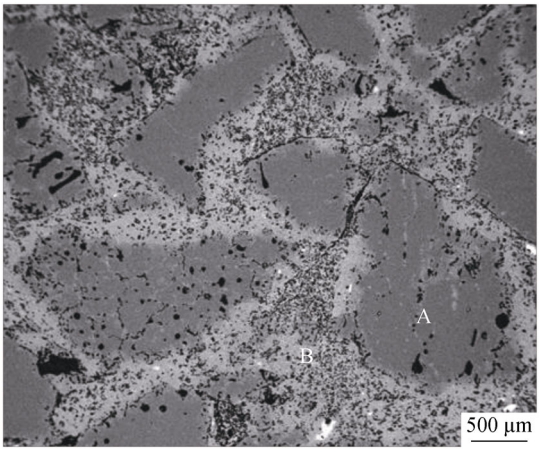

Fig. 1. SEM micrograph of alumina–chromia refractory brick: A—Al_2O_3 aggregate; B—matrix (70wt% Al_2O_3 and 30wt% Cr_2O_3).

2.2. Thermodynamic modeling

Thermodynamic simulations were performed using the FactPS and FToxid databases that accompany the FactSage™ version 6.4 software [17]. The equilibrium phases were predicted for possible phases of gas, slag, and various solid solutions (including corundum, spinel, and mullite) using the Equilib module.

The model used in the present work is illustrated in Fig. 2. According to the proposed model, 100 g of refractory and 100 g of slag were used in the first stage of reaction between these two materials. After the first reaction step, the resulting liquid slag (slag(1)) was again placed into contact with the same amount (100 g) of the original refractory used in the first step and a further thermodynamic calculation was carried out. This procedure was repeated until the calculated amount of the main solid phases reached a constant value.

Because the liquid slag would react with both the matrix and the aggregates while penetrating into the brick, the corrosion behavior between the slag and matrix was thermodynamically simulated first, followed by the behavior between the slag and the surface aggregates and then that between the slag and the inner aggregates. Thus, the "refractory" described in Fig. 2 represents both the matrix and the aggregate. Notably, the resulting slag that penetrates into the aggregates along cracks or pores may combine with the slag along pores in the matrix. However, such a combination is not considered in this calculation. The compositions of the matrix and aggregates of the alumina–chromia refractory are presented in Fig. 1. The compositions of coal slag (CS) and iron smelting slag (ISS) as the corrosion slags used in this work are summarized in Table 1. All calculations were performed for a constant temperature of 1550°C, which approaches the highest service temperature of alumina–chromia refractory brick, under a reducing atmosphere ($P(O_2)$ = 10^{-3} Pa).

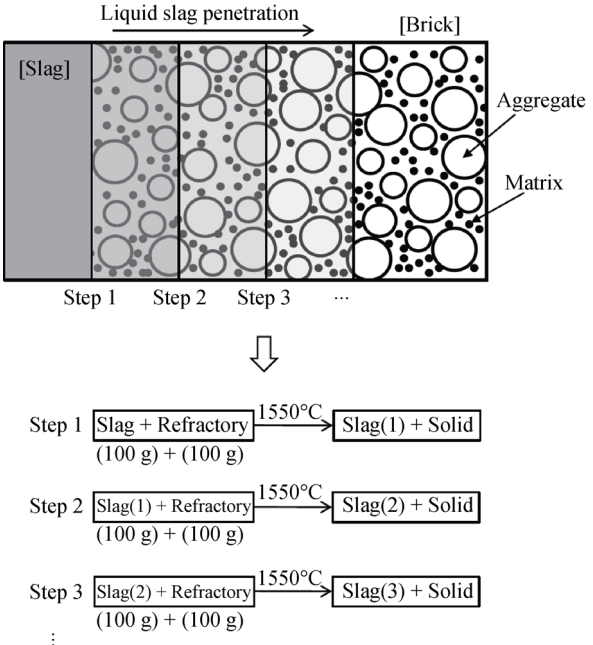

Fig. 2. Simulation model of slag penetration.

Table 1. Chemical compositions of the slags used in this work

wt%

Slags	SiO_2	Al_2O_3	Fe_2O_3	CaO	TiO_2	MgO	Na_2O	K_2O
CS	45.31	20.75	10.41	19.51	0.77	0.89	1.31	1.05
ISS	24.02	11.06	7.33	12.68	24.67	19.54	0.14	0.19

2.3. Corrosion testing procedure

High-temperature corrosion tests were performed in an improved rotary drum furnace. In the testing procedure, a reducing atmosphere could be achieved through adjustment of the molar ratio between ethyne and oxygen as the firing gases. The achievement of a reducing environment was confirmed through analysis of the Fe valence state, which revealed that FeO was the only iron oxide present in the slag. The alumina–chromia refractory bricks were placed into the furnace and heated to 1550°C over a period of 4–5 h. The samples were then corroded for 10 h at 1550°C by the addition of the compositional slags listed in Table 1. The corroded samples were cooled from 1550°C to room temperature inside the furnace. After the experiments, cross sections of the tested samples were analyzed by SEM and energy dispersive spectrometer (EDS) to identify the microstructures, phases, and slag penetration depth.

3. Results and discussion

3.1. Thermodynamic calculations of phase evolution

Fig. 3 shows the phase evaluation after reaction of the refractory brick with CS at different calculation steps. The liquid slag contacts with brick and first reacts with the matrix and surface Al_2O_3 aggregates, which causes obvious alumina dissolution, as observed in Figs. 3(a) and 3(c). Almost no other new phases are formed under these simulation conditions. According to the calculation results, less alumina dissolves at steps 2 and 3, most likely because of saturation of the liquid slag after the first calculation step. Additionally, the calculation results for the further attack on the inner aggregates by the resulting matrix-reacted slag are shown in Fig. 3(b). In this case, the dissolution of alumina is indicated as the main corrosion process, but with a much lower dissolved alumina content, which is also attributed to the nearly saturated liquid slag. The differences in cumulative alumina dissolution for the aforementioned three kinds of reactions are clearly observed in Fig. 3(d).

On the basis of the thermodynamic calculation results, we predict that the dissolving process is likely to be the primary corrosion mechanism when the alumina–chromia brick is attacked by the CS at 1550°C. Liquid slag, Al_2O_3, and Al_2O_3–Cr_2O_3 solution are the main equilibrium phases observed in this reaction system.

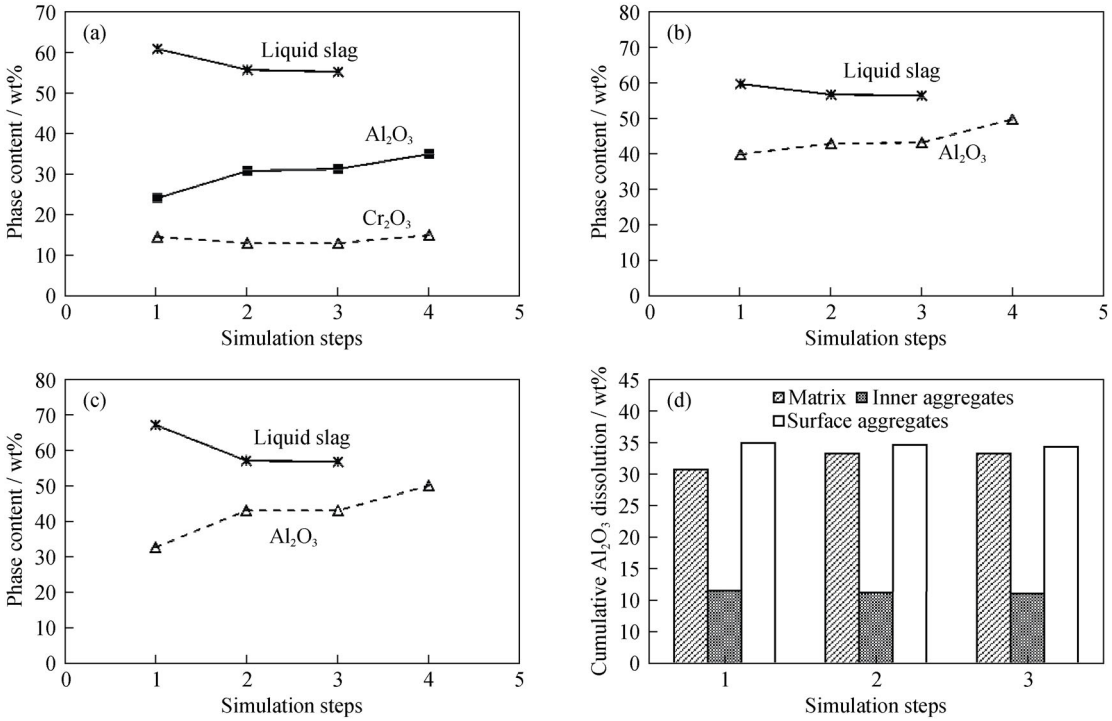

Fig. 3. Phases formed after interactions between CS and the matrix (a), the inner aggregates (b), and the surface aggregates (c) at 1550°C; (d) cumulative Al_2O_3 dissolution into slag at 1550°C.

The calculation results for refractory brick attacked by the ISS are presented in Fig. 4. A remarkably different phase evaluation is obtained in this reaction system. A greater content of liquid slag is present at step 1 when the refractory brick is in contact with the ISS compared to when it is in contact with CS (Fig. 4(a)). Meanwhile, $MgCr_2O_4$ and

$(Mg,Fe)Al_2O_4$ spinel solid phases are formed, possibly because of reactions of the matrix with MgO and FeO in the liquid slag. As the calculation proceeds stepwise, the content of spinel phases decreases and becomes zero at step 12. This result is attributed to the consumption of MgO and FeO in the liquid slag during the simulation steps. Accordingly, the composition of the liquid slag also changes, reaching its saturation point after the long calculation steps. The formed spinel phases at each point contain increasing amounts of $MgCr_2O_4$, which is explained by the observation that the formation of $MgCr_2O_4$ is thermodynamically favored over the formation of $(Mg,Fe)Al_2O_4$ under the present conditions because of the lower Gibbs energy associated with the reaction between MgO and Cr_2O_3 [18]. We also note that $MgAl_2O_4$ is the major phase in $(Mg,Fe)Al_2O_4$. Almost no $FeAl_2O_4$ is observed in the present system because of the low Fe_2O_3 content in the initial slag, similar to the CS. Fig. 4(b) shows the phase evaluation of the inner Al_2O_3 aggregates attacked by the resulting liquid slag after reacting with the matrix. The nearly saturated liquid slag leads to obviously less dissolution of alumina, and no spinel phases are observed due to the consumption of MgO. However, the surface Al_2O_3 aggregates attacked by the original slag could exhibit a different phase composition, as shown in Fig. 4(c). Relatively greater amounts of alumina are dissolved and $(Mg,Fe)Al_2O_4$ spinel phases are formed in this reaction procedure. Similarly, the content of the spinel phase decreases sharply and becomes zero at step 3.

The previous analysis indicates that the ISS can cause greater dissolution of refractory brick into the melt (cumulative alumina dissolution is shown in Fig. 4(d)) compared to the dissolution induced by CS. Moreover, the formation of spinel phases can destroy the main phase structure, which may lead to further corrosion of the refractory brick.

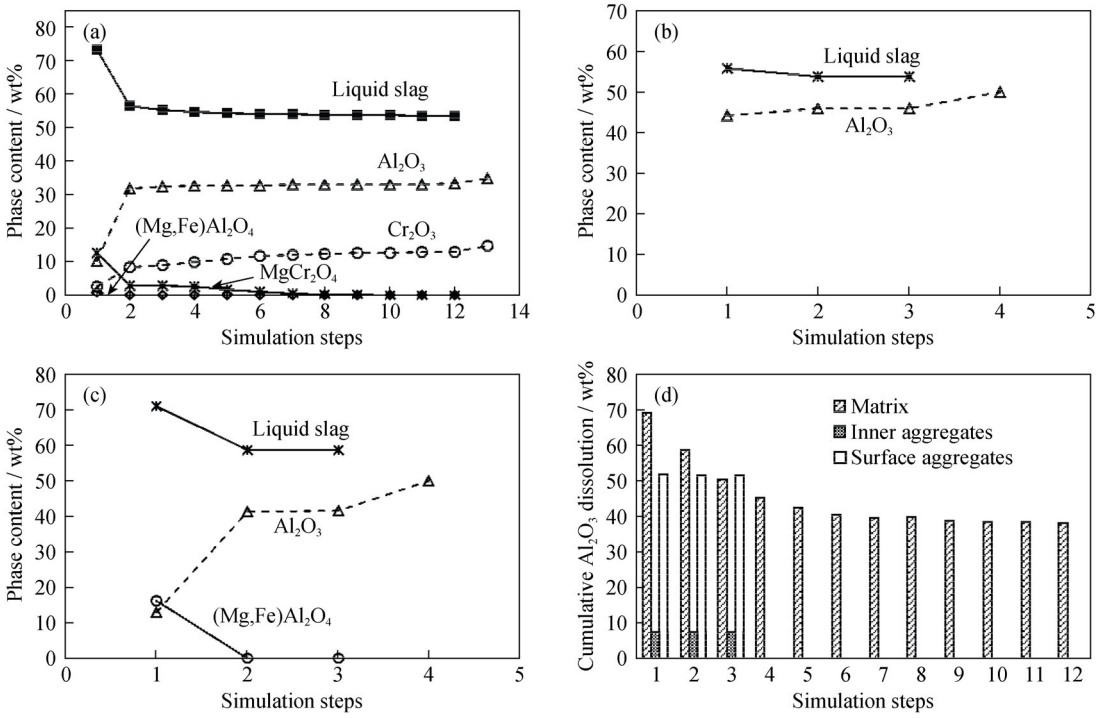

Fig. 4. Phases formed after interactions between the ISS and the matrix (a), the inner aggregates (b), and the surface aggregates (c) at 1550°C; (d) cumulative Al_2O_3 dissolution into the slag at 1550°C.

3.2. Experimental analysis of phase evolution

The cross-section images of alumina–chromia bricks corroded by slags CS and ISS are presented in Fig. 5. The results indicate obviously different corrosion behaviors, where much deeper penetration and severe destruction were induced by the ISS than by the CS. To analyze the different microstructural evolution of corroded samples, a hot area of the surface containing remaining slag was selected and characterized by SEM and EDS.

Fig. 6 shows SEM micrographs of the samples corroded by the CS. The concaves of Al_2O_3 aggregates and matrix (indicated by the white arrow) on the surface of the brick were clearly observed, reflecting the phenomena of dissolution during the process of attack by the molten slag at 1550°C. In addition, only low-melting composites (anorthite, glassy phases, etc.) are detected as the new formed phases on the corrosion surface and in the inner penetration area of

the brick. In addition, small amounts of $Fe(Cr,Al)_2O_4$ spinel are observed at the boundary between the slag and brick. However, given their snow-like morphology and specific location, these spinel phases were not formed at high temperatures; they precipitated in the slag upon cooling.

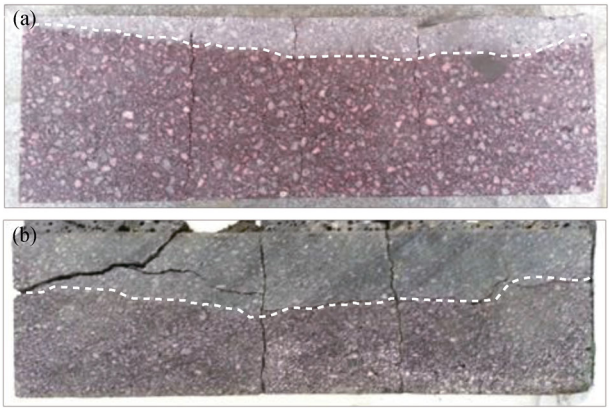

Fig. 5. Cross sections of alumina–chromia bricks after being corroded at 1550°C by CS (a) and ISS (b).

Correspondingly, the microstructure of the refractory brick corroded by the ISS is shown in Fig. 7. A relatively dense product layer containing large amounts of spinel phases is observed in the matrix; this product layer comprises $MgCr_2O_4$ and a small fraction of $(Mg,Fe)Al_2O_4$. Meanwhile, Al_2O_3 aggregates on the surface were completely corroded and tended to form $(Mg,Fe)Al_2O_4$ spinel, although EDS analysis indicated that $MgAl_2O_4$ was the primary phase. Additionally, the amount of spinel phases formed in the matrix gradually decreases with increasing depth into the corrosion brick and becomes zero after a certain depth; this result is consistent with the thermodynamic calculation results shown in Fig. 4(a). Therefore, the phase evaluation of the alumina–chromia refractory brick corroded by slags with different compositions could be simulated by thermodynamic calculations. Further information related to compositional changes as well as liquid viscosity at high temperatures can also be predicted by thermodynamic analysis.

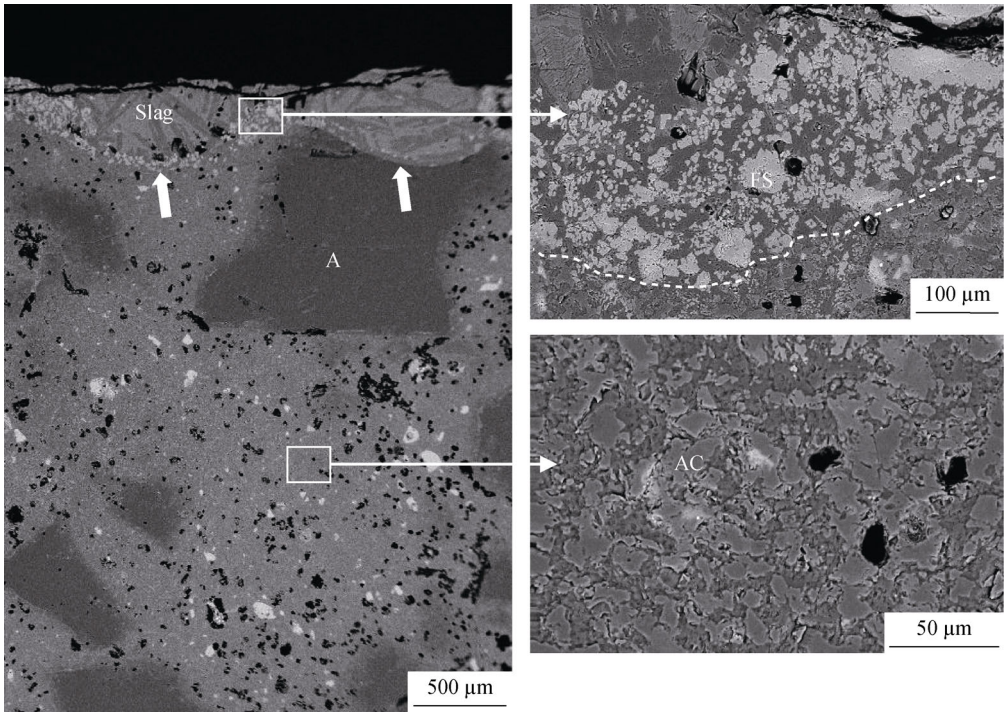

Fig. 6. Corroded sample after interaction with the CS at 1550°C (A—Al_2O_3 aggregate; FS—$Fe(Cr,Al)_2O_4$; AC—Al_2O_3–Cr_2O_3 solid solution).

3.3. Further comparison of experimental and thermodynamic calculation results

To better understand the corrosion process, the results of compositional changes obtained by calculation and experimental analysis are compared in Fig. 8. Notably, the experimental data were only collected for the area from the interaction surface to an inner penetration depth of 5 mm. Both the simulated and experimental results show that the content of main oxides (Si, Ca, and Fe) slowly decreased from the surface to inner space corroded by the CS. The oxide changes confirm the previous analysis indicating that Fe oxides did not react with the refractory to form spinel phases but rather infiltrated into the sample as melts in the liquid

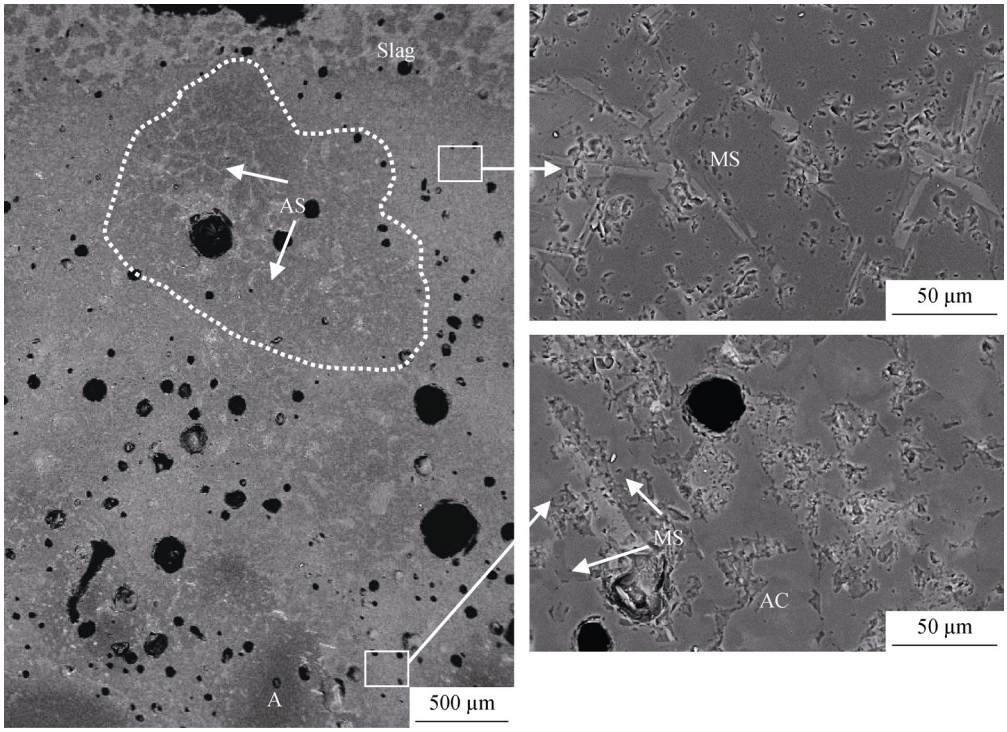

Fig. 7. Corroded sample after interaction with the ISS at 1550°C (A—Al_2O_3 aggregate; AS—$(Mg,Fe)Al_2O_4$; MS—$(Mg,Fe)Al_2O_4$ + $MgCr_2O_4$; AC—Al_2O_3–Cr_2O_3 solid solution).

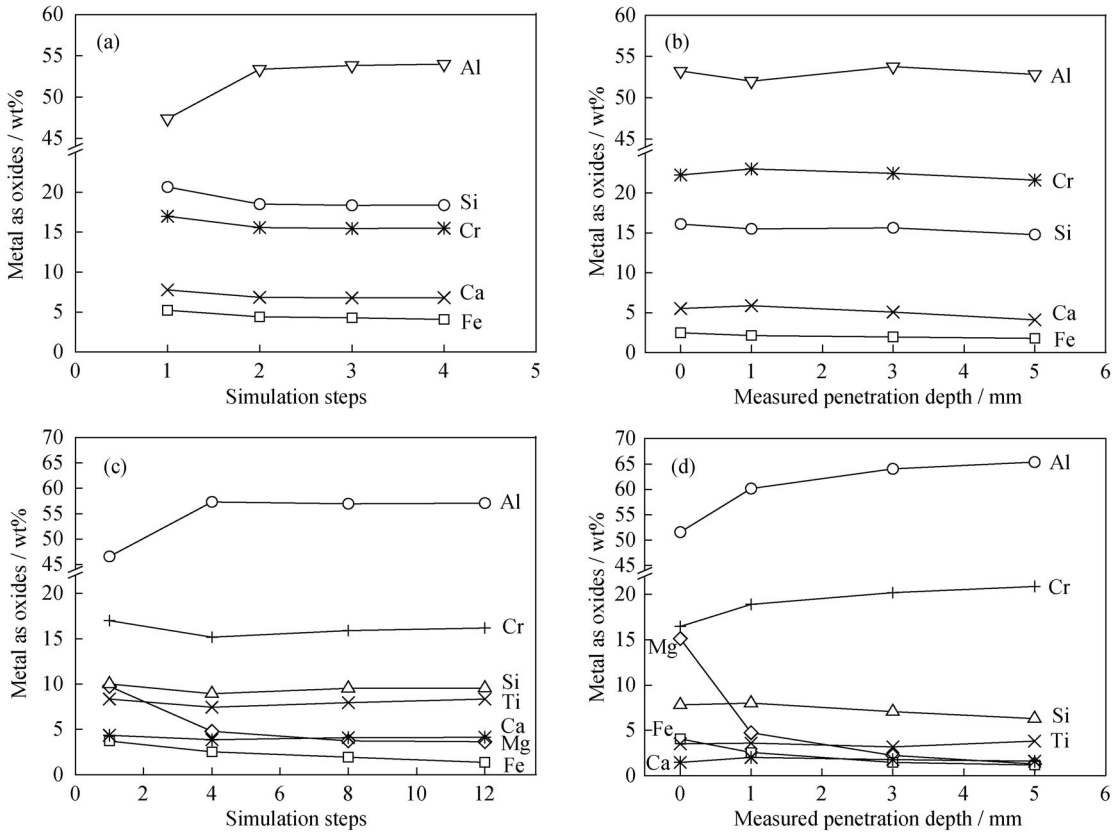

Fig. 8. Simulated and measured mass fraction changes of metal as oxides after interactions between the matrix and CS (a, b) and ISS (c, d) at 1550°C.

slag. In comparison to the interior of the sample attacked by the CS, the interior of the sample attacked by the ISS exhibited a sharp decrease in the content of certain oxides (Mg and Fe), and these oxides were almost absent at a depth of 5 mm. These obvious changes indicate that Mg and Fe oxides were involved in the reaction with the refractory and were mostly consumed on the surface. More importantly, Fig. 8 indicates that the compositional changes and their trends predicted by thermodynamic simulations agree with the experimental results even though some of the values exhibit variance.

Because the results for slag infiltration are very relevant to the results for viscosity, Fig. 9 shows the calculated viscosity changes of slags CS and ISS at high temperatures after their interactions with the refractory brick. The viscosity was estimated using the modified Urbain model, which assumes that all oxides change the liquid viscosity on the sole basis of their own content [19]. The results show that the viscosities of the liquid slags increase with increasing number of simulation steps and tend to become fixed values as the slags approach saturation. In the case of the CS, an increase of the Al_2O_3 content in the liquid phase after each simulation step leads to a slight increase of viscosity at high temperatures. However, the formation of spinel phases and the obvious dissolution of Al_2O_3 upon interacting with the ISS results in a decrease of MgO and FeO contents and an increase in the amount of Al_2O_3 in the liquid phase. Thus, the predicted viscosity for the ISS shows an apparent increase at step 1. Additionally, because of the differences in oxide components, which strongly affect the liquid properties at high temperatures, the ISS exhibits a much lower viscosity compared to that of the CS even after the chemical reaction with refractory brick.

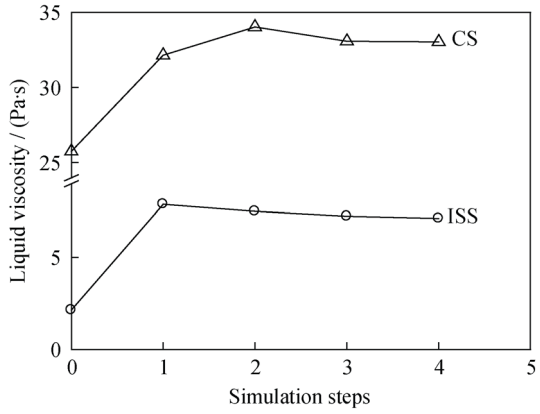

Fig. 9. Calculated viscosities of slags after their interactions with the matrix of the alumina–chromia brick at 1550°C.

On the basis of the calculated viscosities and simulated phase evaluation, deeper slag penetration and more severe corrosion by the attack of the ISS compared to the penetration depth of and corrosion induced by the CS was predicted because of its much lower viscosity and its greater dissolution of alumina; this prediction is confirmed by the experimental results in Fig. 5. Therefore, the present model can be reliable to evaluate the effects of slag chemistry on the corrosion of refractory brick.

Notably, the spinel product layer could be formed on the corrosion surface of the alumina–chromia refractory by the molten slag attack. In general, the formation of this layer depends mostly on the chemical compositions of the slag and on the service conditions. A reducing atmosphere may promote the conversion of Fe^{3+} into Fe^{2+} at high temperatures, which would lead to the formation of spinel phases. However, spinel phases only appeared when the content of Fe_2O_3 and/or MgO reached a certain higher value (as was confirmed by both simulations and experiments in the present research). Moreover, after the spinel phases formed, a relatively dense reaction layer was present on the surface of the sample, which may prevent further liquid infiltration, as suggested by a few researchers [18, 20–21]. However, because of the mismatch of thermal expansion coefficients of spinel phases, cracks might appear inside the dense layer or at the interface between the layer and the refractory, which would likely cause spalling (also observed in the present study in case of the ISS). Therefore, novel spinel formation may exert both positive and negative effects on the corrosion resistance of the alumina–chromia refractory. Further experimental studies are needed to help determine which would be most dominant.

4. Conclusions

(1) The corrosion behavior of two slags on alumina–chromia refractory were investigated via thermodynamic simulations using the proposed model, in which the slag first attacks the matrix and surface aggregates and then attacks the inner aggregates.

(2) On the basis of the simulation results in this work, the slag chemistry strongly affects the phase formation and corrosion of the refractory brick. When the brick was in contact with the ISS, a greater amount of alumina dissolved and newly formed spinel phases were observed compared to when the brick was in contact with the CS.

(3) By referring to the calculated viscosities of molten slags, we predicted that the attack of refractory by the ISS would result in much deeper penetration and more severe corrosion compared to the case of attack by the CS, although the formed product layer in the case of the ISS could inhibit liquid infiltration to some extent. The phase evalua-

tion and compositional changes observed experimentally well matched the predictions.

(4) The agreement between corrosion behavior predicted by thermodynamic simulation and that observed experimentally demonstrates the usefulness of this tool for supporting experimental results. The simulation model presented in this paper appears to be an efficient way to evaluate the different corrosion performances of alumina–chromia refractory upon interaction with various compositional slags.

Acknowledgements

This work was financially supported by the Preliminary Research Project for National Basic Research Program of China (No. 2012CB724607) and the Research Planning Project of Basic and Advanced Technology of Henan Province, China (No.162300410043).

References

[1] T. Hirata, T. Morimoto, S. Ohta, and N. Uchida, Improvement of the corrosion resistance of alumina–chromia ceramic materials in molten slag, *J. Eur. Ceram. Soc.*, 23(2003), No. 12, p. 2089.

[2] T.M. Besmann, N.S. Kulkarni, and K.E. Spear, Thermochemical analysis and modeling of the Al_2O_3–Cr_2O_3, Cr_2O_3–SiO_2, and Al_2O_3–Cr_2O_3–SiO_2 systems relevant to refractories, *J. Am. Ceram. Soc.*, 89(2006), No. 2, p. 638.

[3] M. Nath, K. Dana, S. Gupta, and H.S. Tripathi, Hot corrosion behavior of slip-cast alumina–chrome refractory crucible against molten glass, *Mater. Corros.*, 65(2014), No. 7, p. 742.

[4] D. Chen, A. Huang, H.Z. Gu, M.J. Zhang, and Z.J. Shao, Corrosion of Al_2O_3–Cr_2O_3 refractory lining for high-temperature solid waste incinerator, *Ceram. Int.*, 41(2015), No. 10, p. 14748.

[5] M. Nath and H.S. Tripathi, Thermo-mechanical behavior of Al_2O_3–Cr_2O_3 refractories: Effect of TiO_2, *Ceram. Int.*, 41(2015), No. 2, p. 3109

[6] K. Sekine, Y. Tsuchiya, and H. Kozuka, Improvement of Al_2O_3–Cr_2O_3–ZrO_2 bricks for waste melting kiln, *Taikabutsu Overseas*, 25(2005), No. 3, p. 231.

[7] H.B. Kim and S.O. Myongsook, Changes in microstructure of a high chromia refractory due to interaction with infiltrating coal slag in a slagging gasifier environment, *Ceram. Int.*, 34(2008), No. 8, p. 2107.

[8] M. Freund, Corrosion behaviour of refractory materials in the systems Cr_2O_3 and Cr_2O_3–Al_2O_3 against glass melts in subject to their composition and the thermal conditions, *Refract. World Forum*, 2(2010), No. 3, p. 1.

[9] M. Nath, A. Ghosh, and H.S. Tripathi, Hot corrosion behavior of Al_2O_3–Cr_2O_3 refractory by molten glass at 1200°C under static condition, *Corros. Sci.*, 102(2016), p. 153.

[10] I.H. Jung, Overview of the applications of thermodynamic databases to steelmaking processes, *Calphad*, 34(2010), No. 3, p. 332.

[11] J. Poirier, M.L. Bouchetou, P. Pringent, and J. Berjonneau, An overview of refractory corrosion: observations, mechanisms and thermodynamic modeling, *Refract. Appl. Trans.*, 3(2007), No. 2, p. 2.

[12] J. Berjonneau, P. Prigent, and J. Poirier, The development of a thermodynamic model for Al_2O_3–MgO refractory castable corrosion by secondary metallurgy steel ladle slags, *Ceram. Int.*, 35(2009), No. 2, p. 623.

[13] T.M. Besmann, Thermochemical modeling of refractory corrosion in slagging coal gasifiers, *Calphad*, 32(2008), No. 3, p. 466.

[14] M.K. Cho, M.A. Van Ende, T.H. Eun, and I.H. Jung, Investigation of slag-refractory interactions for the Ruhrstahl Heraeus (RH) vacuum degassing process in steelmaking, *J. Eur. Ceram. Soc.*, 32(2012), No. 8, p. 1503.

[15] M. Reinmöller, M. Klinger, E. Thieme, and B. Meyer, Analysis and prediction of slag-induced corrosion of chromium oxide-free refractory materials during fusion of coal and biomass ash under simulated gasification conditions, *Fuel Process. Technol.*, 149(2016), p. 218.

[16] B. Long, B. Andreas, and G.Y. Xu, Thermodynamic evaluation and properties of refractory materials for steel ladle purging plugs in the system Al_2O_3–MgO–CaO, *Ceram. Int.*, 42(2016), No. 10, p. 11930.

[17] C.W. Bale, E. Bélisle, P. Chartrand, S.A. Decterov, G. Eriksson, K. Hack, I.H. Jung, Y.B. Kang, J. Melançon, A.D. Pelton, C. Robelin, and S. Petersen, FactSage thermochemical software and databases: recent developments, *Calphad*, 33(2009), No. 2, p. 295.

[18] T.K. Kaneko, J.X. Zhu, N. Howell, P. Rozelle, and S. Sridhar, The effects of gasification feedstock chemistries on the infiltration of slag into the porous high chromia refractory and their reaction products, *Fuel*, 115(2014), p. 248.

[19] G.J. Browning, G.W. Bryant, H.J. Hurst, J.A. Lucas, and T.F. Wall, An empirical method for the prediction of coal ash slag viscosity, *Energy Fuels*, 17(2003), No. 3, p. 731.

[20] J.P. Bennett and K.S. Kwong, Failure mechanisms in high chrome oxide gasifier refractories, *Metall. Mater. Trans. A*, 42(2011), No. 4, p. 888.

[21] H. Wang, H.Q. Lan, K.M. Geng, S.P. Lü, and X. Fang, Corrosion resistance of fused Cr_2O_3–Al_2O_3 grains materials with different compositions in Cr_2O_3–Al_2O_3 bricks, *Refractories*, 44(2010), No. 6, p. 442.